JOURNAL OF MATERIALS SCIENCE **35** (2000) 3279–3287

Preparation of $x\mathrm{TiO_2}\cdot(1-x)\mathrm{Al_2O_3}$ catalytic supports by the sol-gel method: physical and structural characterisation

R. LINACERO, M. L. ROJAS-CERVANTES*, J. DE D. LÓPEZ-GONZÁLEZ
Departamento de Química Inorgánica y Química Técnica, Facultad de Ciencias (U.N.E.D.), Paseo Senda del Rey nº 9, Madrid 28.040, Spain
E-mail: mrojas@ccia.uned.es

A series of $x\mathrm{TiO_2}\cdot(1-x)\mathrm{Al_2O_3}$ mixed oxides has been prepared by the sol-gel method with variable amounts of $\mathrm{TiO_2}$, from pure alumina to pure titania. Textural, bulk and surface characterisation of the samples has been carried out by nitrogen physisorption (S_{BET}, porosity), thermal analysis (TGA, DTA), X-ray diffraction (XRD), zero point charge (ZPC) and surface acidity. The textural results show that at low titania contents, higher surface areas than those of pure alumina are obtained, and in the titania-rich samples, higher surface areas than for pure titania are stabilised. The titanium content also affects the crystallization process. Furthermore, the strength and distribution of the acid sites may be varied by changing the composition of the mixed oxide.

1. Introduction

One of the most important applications of the sol-gel method can be found in the field of catalysis. The high porosity of the gels together with the great number of disposable surface OH groups, make them very attractive from the catalytic point of view. On the other hand, it is well known that in many catalytic systems, the performance depends not only on the nature and structure of the active phase, but also on the chemical and structural characteristics of the support, although there is a debate about the interpretation of this fact [1–3].

The sol-gel method not only allows a good control of the characteristics of the support, but also offers the possibility of preparing a supported oxide catalyst from a homogenous solution containing both the metal precursor and the support precursor [4–7].

Each step of the process can be controlled and modified in order to obtain a specific material exhibiting a good and adequate catalytic behaviour. Thus, some authors have found that the catalysts prepared by the sol-gel method show higher activity for hydrodesulfuration reactions than those prepared by conventional methods [8, 9].

On the other hand, hydroprocesing catalysts prepared with alternative supports can sometimes have higher sulphur and nitrogen removal activities when compared with conventionally prepared alumina supported catalysts. Thus, Weissman *et al.* [10] found that titania-zirconia mixed oxide aerogels with high content of $\mathrm{TiO_2}$, while somewhat unstable, were more active on a surface area basis than $\mathrm{Al_2O_3}$ or conventional $\mathrm{TiO_2}$ equivalent supported Mo-Ni catalysts, finding that the support acidity contributes to hydrotreating activity. Besides, when $\mathrm{TiO_2}$ was used as a support for Mo and CoMo or NiMo hydrotreating catalysts, the presulfiding process was not necessary for activation [11]. However, the disadvantage of titania as support is that it is unsuitable for industrial applications because of its relatively low surface area and the poor stability of the active anatase structure at high temperatures. Therefore, much attention has been paid to the applications of mixed oxides containing titania [12–15]. In this line, the use of alumina-titania mixed oxides supports seems to be a good alternative to overcome the problems of the poor sulfidation shown by the alumina supported catalysts and the low surface area of those supported on titania [16].

Considering all the above exposed, and taking into account our previous experience about the synthesis of supports and supported catalysts by the sol-gel method [7, 9, 17, 18] in the present paper we report the synthesis of the $x\mathrm{TiO_2}\cdot(1-x)\mathrm{Al_2O_3}$ series with different molar ratios. The use of well characterised titania-alumina mixed oxides will allow us to tune the chemical and textural surface properties of the support, by changing the ratio of the two oxides and, in this way, to be able to design better and more selective catalysts. Characterisation of the final $\mathrm{TiO_2}$-$\mathrm{Al_2O_3}$ solids obtained by sol-gel procedure is necessary in view that the alkoxide precursor hydrolyses at rates which are dependent on the precursors. Clearly, the simultaneous hydrolysis, condensation and gelation of the Ti and Al species are complex, and therefore one

* Author to whom correspondence should be addressed.

would expect different behaviours in the preparation of mixed oxides with different Ti/Al ratios.

In the present paper, the first of a series on TiO_2-Al_2O_3 mixed oxides as supports for hydrotreatment catalysts, we present the results from the structural (XRD), textural (surface area, pore size and pore volume distributions) and physicochemical (zeta potential, thermal analysis, surface acidity) characterisation of TiO_2-Al_2O_3 mixed oxides with varying amounts of titania prepared by the sol-gel method. These supports will be used in a subsequent work as supports for hydrotreatment Mo based catalysts.

2. Experimental

2.1. Synthesis

A series of sol-gel $x\mathrm{TiO_2}\cdot(1-x)\mathrm{Al_2O_3}$ with different molar ratios $x = \mathrm{TiO_2}/(\mathrm{TiO_2} + \mathrm{Al_2O_3})$ were prepared ($x = 0.0$, 0.2, 0.5, 0.6, 0.8 and 1.0). In all cases, *n*-propanol, water and nitric acid were used as solvent, hydrolysing agent and catalyst, respectively, and the molar ratios used for the synthesis were H_2O/alkoxide $= 5$, propanol/alkoxide $= 15$ and HNO_3/alkoxide $= 0.2$.

The general procedure was as follows. Aluminium isopropoxide (IsopAl) was dissolved slowly in 83% of the total *n*-propanol, calculated for each formulation according with the molar ratios given above. Heating under reflux and stirring for 3 h was necessary for a complete dissolution. Once the aluminium isopropoxide was dissolved and cooled at room temperature, the appropriate amount of titanium isopropoxide (IsopTi) to produce the designed mixed oxide formulation was added. After that, a mixture of the remaining 17% *n*-propanol and the necessary water to maintain the H_2O/alkoxide $= 5$ ratio was added dropwise under continuous stirring. The solution gelled in all cases before adding the total amount of that solution, except in the case $x = 1.0$, which gelled 3 minutes after the addition of the last drop. Taking into account the added volume, the molar ratios necessary to produce the gel were calculated and they are shown in Table I. It can be observed that when the molar ratio x in the mixed oxides increases, the molar ratios H_2O/alkoxide, *n*-propanol/alkoxide and acid/alkoxide necessary to form the gel also increase, up to the values of 5, 15 and 0.2, respectively, for the TiO_2 precursor. However, although the gellification occurred before, the totality of the solution was added in all cases, to keep constant the initial molar ratios. The gel was aged for 3 days, afterwards a sensible shrinking was observed, and the supernatant liquid was removed. The samples were then dried in an atmospheric oven at 80 C for 14 hours and calcined at 500 C under an air flow of 75 mL·min^{-1} using the following calcination program:

$$T_0 = 30\ \mathrm{C}$$
$$r_1 = 3\ \mathrm{C\cdot min^{-1}} \quad T_1 = 100\ \mathrm{C} \quad t_1 = 30\ \mathrm{min}$$
$$r_2 = 3\ \mathrm{C\cdot min^{-1}} \quad T_2 = 300\ \mathrm{C} \quad t_2 = 60\ \mathrm{min}$$
$$r_3 = 3\ \mathrm{C\cdot min^{-1}} \quad T_3 = 500\ \mathrm{C} \quad t_3 = 180\ \mathrm{min}$$

TABLE I Molar ratios necessary to produce the gel in the $x\mathrm{TiO_2}\cdot(1-x)\mathrm{Al_2O_3}$ series

Sample	H_2O/alkoxide	*n*-propanol/alkoxide	acid/alkoxide
$x = 0.0$	2.00	13.52	0.069
$x = 0.2$	1.21	13.09	0.029
$x = 0.5$	1.37	13.13	0.057
$x = 0.6$	2.95	13.92	0.120
$x = 0.8$	4.93	14.92	0.197
$x = 1.0$	5.00	15.00	0.200

3. Characterisation techniques

Thermal gravimetry and differential thermal analyses (TG-DTA) were carried out in a Seiko SSC 5200 TG-DTA 320 System under an air flow of 75 mL·min^{-1}, with a heating rate of 5 C·min^{-1}. The BET surface areas and the pore volume distributions were measured by nitrogen adsorption at 77 K in a MICROMERITICS ASAP 2000 equipment. The X-ray powder diffraction patterns were measured and evaluated with a Seifert C-3000 diffractometer, using Cu-K_α radiation with a secondary monochromator. The measurements of zeta potential were carried out in a zeta meter 3.0^+ instrument using 125 mg of sample dispersed in 25 mL of water as pattern solution. From this dispersion, 2 mL were diluted with 98 mL of distilled water, and they were used to prepare a diluted dispersion with a solid concentration of 100 ppm. The pH was adjusted with either NaOH or HCl solutions and measured with a Tritio DMS 716 pH meter. The solutions were kept for 12 hours to reach the equilibrium pH before measuring the Zeta potential, which was obtained from electophoretic migration rates using the Smoluchowski equation. A potentiometric method of titration with *n*-butylamine was used to characterize the surface acidity. With this method, the total number of surface acid centres and the relative maximum acid strengths of the initially titrated surface sites of the prepared solids are determined [19]. A small quantity (0.2 mL) of 0.2 N *n*-butylamine in acetonitrile was added to 0.15 g of solid and kept under stirring for 3 hours. According to the method used, the initial electrode potential indicates the maximum acid strength of the first titrated surface acid sites. The titration of the suspension was continued with the same base using volume increments of 0.1 mL, and a waiting time of 30 s for each potential measurement. The total number of acid sites was estimated from the total amount of base added to reach the plateau in the potential vs. volume curve. A polar solvent (acetonitrile) was chosen in order to avoid the problem of the irreversible adsorption of *n*-butylamine on an inert solvent [20]. Further details of the method can be found in Ref. [19]. The electrode potential during the titration was registered on a Tritio DMS 716 digital pHmeter with a combined glass and Ag/AgCl electrode.

4. Results and discussion

4.1. Surface and pore size distribution

The textural characteristics of the dried and calcined samples are given in Table II. Together with the BET surface areas (S_{BET}), the micropore surfaces (S_{MIC}) calculated from *t*-plot method [21] and the cumulative meso [22] and micropore [23] volumes are given.

TABLE II Textural characteristics of dried and calcined samples of the $x\mathrm{TiO_2}\cdot(1-x)\mathrm{Al_2O_3}$ series

	Dried samples (80 C)				Calcined samples (500 C)			
Sample	S_{BET} (m^2/g)	S_{MIC} (m^2/g)	V_{BJH} (cm^3/g)	V_{HK} (cm^3/g)	S_{BET} (m^2/g)	S_{MIC} (m^2/g)	V_{BJH} (cm^3/g)	V_{HK} (cm^3/g)
$x=0.0$	633	186	0.413	0.237	296	—	0.430	0.114
$x=0.2$	165	147	0.018	0.068	361	98	0.221	0.128
$x=0.5$	256	222	0.034	0.106	300	132	0.124	0.109
$x=0.6$	85	72	0.014	0.035	178	—	0.248	0.066
$x=0.8$	319	274	0.044	0.129	142	—	0.228	0.053
$x=1.0$	259	232	0.024	0.109	14	—	0.037	0.005

V_{BJH}: mesopore cumulative volume (20–500 Å) from BJH adsorption branch; V_{HK}: micropore volume (<20 Å) from Horvath-Kawazoe.

The surface areas of the precursors (gels dried at 80 C) are in the range 85–633 m^2/g, although a clear trend of the area evolution with the TiO_2 molar ratio (x) is not observed. The S_{BET} and S_{MIC} values are very similar (except in the case $x=0.0$), which indicates that the contribution to the area is fundamentally due to the micropores, that is, the samples are more microporous than mesoporous. This is also corroborated by comparing the values of BJH mesopore volumes (V_{BJH}) with Horvath-Kawazoe micropore volumes (V_{HK}) values. It is observed that the second are 3–5 times higher than the first ones, with the exception of $x=0.0$ sample, which contains a mesoporous volume approximately double that the microporous volume.

When the samples are calcined at 500 C, an increase of the S_{BET} values is originated with respect to those of the precursors for samples of intermediate composition (see Table II), fundamentally due to a development of the mesoporosity in these samples. The major contribution to the S_{BET} comes from the mesopores, since the values of S_{MIC} obtained by the calculation program are negative (indicating the absence of microporous) or much lower than the values of S_{BET} ($x=0.2$ and $x=0.5$ samples). The calcination process leads probably to the removal of a great part of the organic groups occluded into the pores of the gel, resulting in the accessibility of these to the nitrogen molecules. Thus, the mesopore volume values (V_{BJH}) are much higher than the micropore volume ones (V_{HK}), specially in the samples with higher titanium content (see Table II).

When the samples calcined contain titanium in low molar ratios, an increment of the S_{BET} value is produced with respect to that of pure alumina, occurring then a progressive decrease from the $x=0.5$ sample down to the lowest value ($S_{BET}=14$ m^2/g), for the sample containing only titania. These results agree satisfactorily with the ones obtained by Klimova *et al.* [24] who found an increase of the S_{BET} with the molar ratio until $x=0.5$ and a posterior decrease for higher x values in samples $x\mathrm{TiO_2}\cdot(1-x)\mathrm{Al_2O_3}$ prepared using ammonium carbonate as chemical additive to modify the porosity. Similarly, these authors observed that the addition of ZrO_2 to the alumina in a molar ratio of $x=0.2$ increased slightly the surface area, occurring a decrease when more zirconia was added [18]. On the contrary, other authors [25] found the maximum of the surface area for the ratio $x=0.8$ in $x\mathrm{TiO_2}\cdot(1-x)\mathrm{Al_2O_3}$ supports calcined at 500 C, while Toba *et al.* [26] observed a progressive decrease of the area with the titanium content in alumina-titania samples prepared by different sol-gel methods. We have obtained, in general, S_{BET} values higher than others reported previously for samples prepared by sol-gel methods. Thus, the S_{BET} values for $x=0.0$, $x=0.5$ and $x=1.0$ obtained by us are higher (approximately in a factor of 1.5) than the found by other authors [27]. The S_{BET} value for the $x=0.5$ sample is 3.5 times higher than the found by Lee and Lee [28] in a sample Al_2O_3-TiO_2 of the same molar ratio prepared by mixture of the two sols calcined at 500 C. Besides, the S_{BET} values for $x=0.2$ and $x=0.5$ samples are comprised between the reported by Toba *et al.* [26] for these samples prepared by complexing agent assisting sol-gel method and the ones of the same samples prepared by a coprecipitation method.

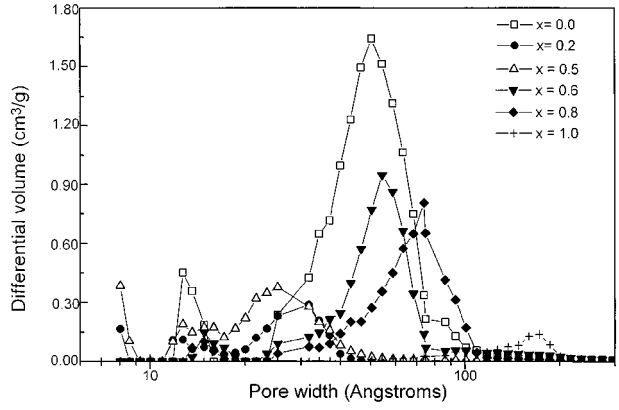

Figure 1 DFT distributions of the samples of the $x\mathrm{TiO_2}\cdot(1-x)\mathrm{Al_2O_3}$ series calcined at 500 C.

The pore size distributions of the calcined samples obtained by applying the Density Functional Theory (DFT) [29] are shown in Fig. 1. The sample containing only alumina ($x=0.0$) presents the maximum around 50 Å and a very similar distribution to those of some aluminas prepared by Balakrishnan and Gonzalez [5]. When the titanium content increases until $x=0.5$, the curves are shifted to the left, that is, smaller pore diameters are obtained. However, if the titanium amount continues increasing above $x=0.5$, a shift to higher pore sizes is produced, in such way that the sample containing only titania ($x=1.0$) presents a maximum around 170 Å. Klimova *et al.* [18] observed, on the contrary, a progressive decrease of the pore sizes with an increase of x in $x\mathrm{ZrO_2}\cdot(1-x)\mathrm{Al_2O_3}$ samples.

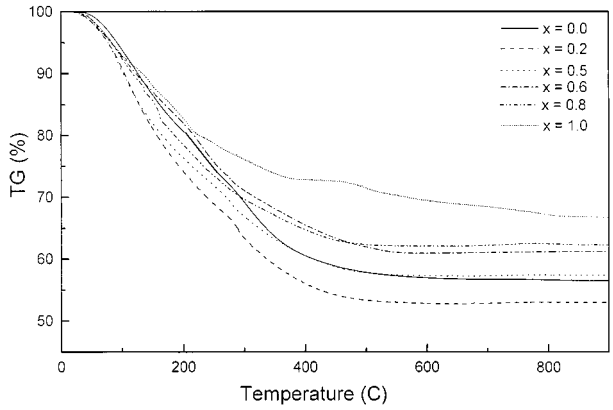

Figure 2 TG curves of the precursors of the $x\mathrm{TiO_2}\cdot(1-x)\mathrm{Al_2O_3}$ series dried at 80 C.

TABLE III Temperature (C) of the maxima of DTA curves for the precursors of the $x\mathrm{TiO_2}\cdot(1-x)\mathrm{Al_2O_3}$ series and for IsopTi and IsopAl

Sample	Temperature (C)					*
IsopTi	—	234(endo); 243	—	374	—	765
IsopAl	140(endo)	—	281	—	—	836; 854
$x=0.0$	—	209; 227	291; 314	—	—	845
$x=0.2$	—	260	281; 290	—	—	862
$x=0.5$	—	261	281	—	—	769
$x=0.6$	—	263	271	—	—	696
$x=0.8$	158	262	—	353	420	655
$x=1.0$	146	246	—	—	413	498

All the peaks are exothermic, if the opposite is not indicated.
*Temperature associated with the crystallization process or phase transformation.

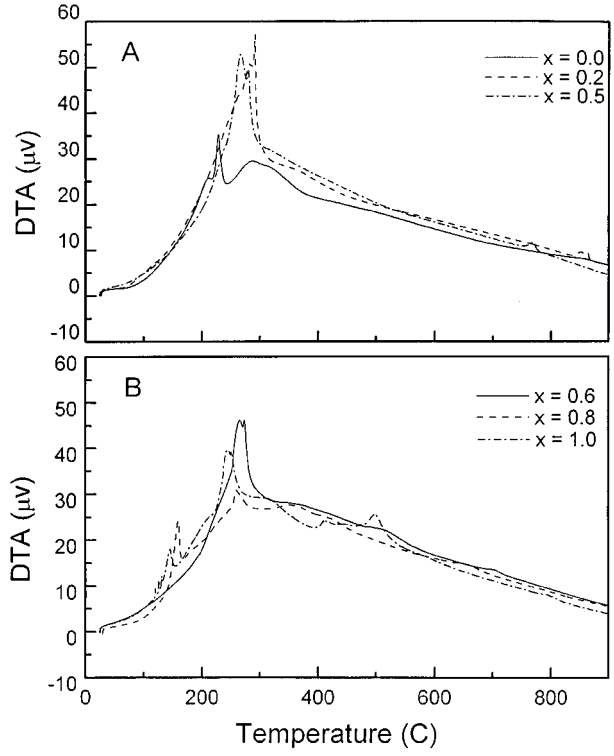

Figure 3 DTA curves of the precursors of the $x\mathrm{TiO_2}\cdot(1-x)\mathrm{Al_2O_3}$ series dried at 80 C. A) $0.0 \leq x \leq 0.5$; B) $0.6 \leq x \leq 1.0$.

4.2. Thermal behaviour

The thermogravimetric analyses of the samples of the $x\mathrm{TiO_2}\cdot(1-x)\mathrm{Al_2O_3}$ series, dried at 80 C, are shown in Fig. 2. The samples show a residue value comprised between 56.6 and 67.0 wt %. It can be observed that the higher the titanium content of the sample, the lower is the weight loss, with the exception of the sample $x=0.2$, which is the one showing the lowest residue value. A similar behaviour was observed by Klimova *et al.* [18] for $x\mathrm{ZrO_2}\cdot(1-x)\mathrm{Al_2O_3}$ precursors, where the weight loss increased until $x=0.5$, diminishing with the addition of higher titanium amounts. In general, we have observed weight losses higher than others reported in the literature, which could indicate that the polimerization has been produced in a lower extension in our case. Thus, the sample containing equal amounts of $\mathrm{TiO_2}$ and $\mathrm{Al_2O_3}$, that is, $x=0.5$, shows a weight loss (42.7 wt %) a little bit higher than that found by Lee and Lee [28] for a sample with the same molar ratio, prepared by mixing of the two corresponding sols. Besides, the sample containing only titania ($x=1$) experiments a weight loss (33 wt %) higher than the observed by Montoya *et al.* [30] in several $\mathrm{TiO_2}$ samples, in which the weight losses were comprised between 14.6 and 27.0 wt %, depending on the type of alcohol used as solvent.

The complexity of the aluminium-titanium polymeric system formed by the hydrolysis process makes difficult the assignment of a step of the TG curve to the removal of a particular component. It must be taken into account that in the precursor gel many different components can exist, such as structures with hydroxide and oxygen bridges, physical and chemically bound alcohol molecules, adsorbed water, esters groups, etc. Thus, some well-differentiated weight losses are not observed, but a continue loss due to the overlapping of the different decomposition processes. However, three weight loss steps can be noticed in the derivative curves (not shown for simplicity). There is a first zone up to around 210–220 C, assigned to the removal of physisorbed water and propanol. The second step up to around 300 C, slower than the first one, is associated with the pyrolysis of the organic groups since it is well corresponded with the exothermic peaks due to the loss of the alkoxide groups in both aluminium isopropoxide and titanium isopropoxide (see decomposition temperature for both alkoxides in Table II). Additionally, there is a third weight loss step from 300 C onwards, which presumably corresponds to the water lost during the formation of the oxide. These results are in agreement with the ones reported by other authors for $x\mathrm{TiO_2}\cdot(1-x)\mathrm{Al_2O_3}$ supports [18].

The DTA curves for the $x\mathrm{TiO_2}\cdot(1-x)\mathrm{Al_2O_3}$ series are depicted in Fig. 3, and the temperatures of the maxima for the observed peaks are given in Table III together with the corresponding ones to the raw alkoxides. In most of the samples (all having intermediate compositions) there is a double exothermic peak in the 260–290 C temperature range. The first one, centred at about 263 C, corresponds to the titanium isopropoxide decomposition, and the second one, near 282 C, is assigned to the exothermic decomposition observed in the aluminium isopropoxide. It can be noticed that this

double peaks shifts to the left when the titanium content increases, due to the lower decomposition temperature of the titanium alkoxide (243 C) with respect to that of aluminium alkoxide (281 C). Additionally, a broad and weak exothermic peak, centred at 350 C, is observed for the sample $x = 0.8$, corresponding to the peak centred at 374 C detected in the DTA curve of IsopAl, which is associated with the crystallization process of an amorphous phase into anatase TiO_2. This peak is not observed for samples with molar ratios $x < 0.8$. The DTA curve for the sample $x = 1.0$ shows an exothermic peak near 250 C, corresponding to the IsopTi decomposition and other two peaks at 413 C and 498 C. These two peaks could be also associated with the formation of a crystalline phase from the amorphous precursor or with a phase transformation since they correspond to a constant weight region in the TG curve. The same type of assignment could be done for the peaks centred at 695, 768 and 860 C for the $x = 0.6$, 0.5 and 0.2 samples, respectively. Thus, this high temperature peak in the DTA curves corresponds to the crystallization of different aluminium and titanium phases, as will be discussed in the following section.

4.3. Crystalline phases

A detailed study of the crystalline phases formed during the calcination process is of a great importance, because the nature of the crystalline phases can affect the catalytic behaviour of the support. Thus, for example, the anatase-to-rutile phase transformation is considered to represent the major factor in catalytic deactivation in selective oxidation catalysts [31–33].

The precursors dried at 80 C are amorphous, as detected in their corresponding diffraction patterns (not shown here). As observed in the diffractograms of the samples calcined at 500 C (depicted in Fig. 4), the samples corresponding to the $0.0 \leq x \leq 0.6$ composition range are amorphous, meanwhile the diffractograms of the $x = 0.8$ and $x = 1.0$ samples reveal the presence of anatase and a mixture of anatase and rutile, respectively. Thus, any diffraction peak assignable to a crystalline phase containing titanium is observed for samples of $x < 0.8$ molar ratios, that is, in these samples the titanium must be very dispersed forming very small crystallites, whose size is not large enough to be detected by DRX. This result is in agreement with the ones reported by Ramirez and Gutierrez-Alejandre [27] for TiO_2-Al_2O_3 supports, where anatase crystals were not detected for samples of $x < 0.7$ composition. These authors also found that the incorporation of titania seemed to decrease the crystallinity of the γ-Al_2O_3 with respect to the one corresponding to pure alumina, in such way that the diffractograms of $x = 0.5$ and $x = 0.7$ samples were amorphous. In our case, not only the samples with intermediate composition are amorphous, but the alumina pure support ($x = 0.0$) is also amorphous. The differences observed in this sample could be due to the different calcination conditions, because those authors calcined the samples at 500 C for 24 h and in our case the calcination time at that temperature was only 3 h. As indicated above, the difractogram of the $x = 1.0$ sample shows a mixture of anatase and rutile phases. As discussed before, an exothermic peak centred at 413 C was observed in the DTA curve of this sample, associated with the crystallization process of anatase, and another peak centred at 498 C was also observed, corresponding to the transformation of anatase into rutile. The proximity of this last temperature to the calcination temperature (500 C) could be the reason why the phase transformation process has not finished completely, which justifies the presence of the two phases in the difractogram. The crystallization temperature of anatase is close to that observed by other authors in the case of the crystallization of titanium oxides prepared by a sol-gel method, although in different conditions [30] to ours. Likewise, the presence of a mixture of anatase and rutile (97% and 3%, respectively) was detected by other authors in the diffractograms of titanium oxides prepared by the sol-gel method and calcined at 400 C [25]. Shuo *et al.* [34] found a proportion of 85 and 15% for anatase and rutile, respectively, in a TiO_2 prepared from hydrolysis of titanium isobutoxide and calcined at 600 C for 5 hours. A similar proportion was found by Fu *et al.* [35] (90% anatase, 10% rutile) in samples calcined at 300 C, the rutile becoming predominant respect the anatase if the samples were calcined at 500 C. In our case, the rutile fraction was determined from the intensities of the [101] and [110] reflections planes for anatase (I_A) and rutile (I_R), respectively, by applying the formula $x_R = 1 / [1 + 1.26\ (I_A/I_R)]$ [36]. We have obtained a proportion of 43 and 57% for anatase and rutile, respectively. On the other hand, as indicated before, the difractogram of the sample $x = 0.8$ calcined at 500 C shows the presence of anatase. As an exothermic peak was observed at 655 C (see Table III) in the corresponding DTA, it was decided to calcine this sample to a temperature higher than 655 C, in order to check if that peak could correspond to the anatase-to-rutile transformation. However, this last phase was not detected in the difractogram of the sample calcined at 725 C, and only the anatase phase was detected, probably because of the different conditions used during the calcination process and the DTA experiments.

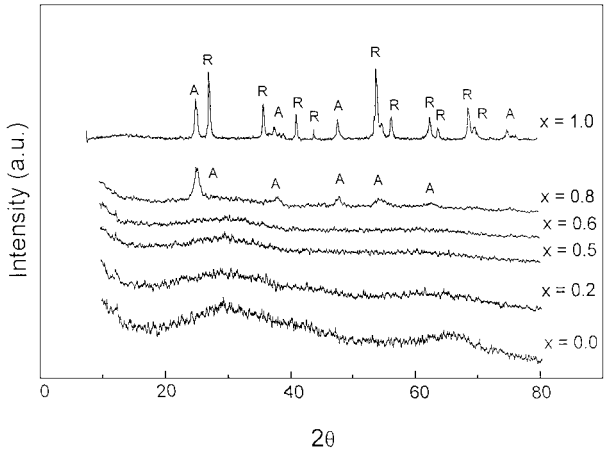

Figure 4 X-ray diffraction patterns of the samples of the $x TiO_2 \cdot (1-x)Al_2O_3$ series calcined at 500 C. A: anatase; R: rutile.

As discussed in the previous section, the crystallization process seems to occur at temperatures above

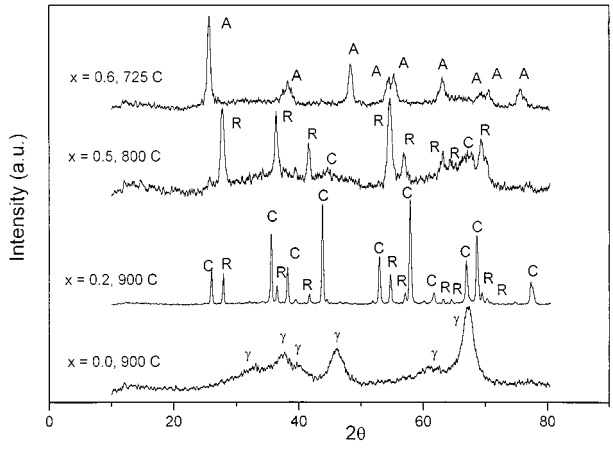

Figure 5 X-ray diffraction patterns of the samples of the $x\text{TiO}_2\cdot(1-x)\text{Al}_2\text{O}_3$ series calcined at different temperatures. A: anatase; R: rutile; C: corundum (α-Al_2O_3); γ: γ-Al_2O_3.

500 C for the $0.0 \leq x \leq 0.6$ samples. These samples were calcined at higher temperatures, chosen in function of the ones observed in the corresponding DTA curves (see Table III). The diffractograms of these samples calcined at different temperatures are shown in Fig. 5. As noticed in the diffractograms, all the samples are crystalline, in such way that the temperatures of the DTA peaks marked with an asterisk in the Table III are associated with crystallization processes. The samples rich on aluminium ($x = 0.0$, $x = 0.2$) contain crystalline phases of aluminium compounds while the diffractograms of the samples with high molar ratios of TiO_2 show only the presence of titanium compounds. Thus, the hexagonal phase of γ-Al_2O_3 with a low degree of crystallinity is detected for $x = 0$ sample, and a mixture of α-Al_2O_3 (corundum) and rutile is observed for $x = 0.2$ sample.

The phase transitions of the alumina, which have been studied for decades [37, 38] show always the same sequences:

$$\gamma\text{-boehmite} \xrightarrow{400\ \text{C}} \gamma\text{-Al}_2\text{O}_3 \xrightarrow{750\ \text{C}} \delta \xrightarrow{900\ \text{C}} \theta \xrightarrow{1200\ \text{C}} \alpha\text{-Al}_2\text{O}_3$$

$$\text{gibsite} \xrightarrow{250\ \text{C}} \chi\text{-Al}_2\text{O}_3 \xrightarrow{500\ \text{C}} \kappa\text{-Al}_2\text{O}_3 \xrightarrow{1000\ \text{C}} \alpha\text{-Al}_2\text{O}_3$$

In spite of the formation of γ-Al_2O_3 from γ-boehmite described in these sequences occurs around 400 C, in our case, as the raw material is not the boehmite and the calcination conditions are different, the γ-Al_2O_3 is not obtained by us for the sample $x = 0$ until this is calcined at 900 C. On the other hand, the transformation into α-Al_2O_3 occurring at 1200 C for the pure alumina is observed by us at temperatures below 900 C for the $x = 0.2$ sample, as noticed in the corresponding difractogram (see Fig. 5), which shows the presence of corundum (α-Al_2O_3). Thus, the sample $x = 0.0$ calcined at 900 C contains the γ-Al_2O_3 phase, meanwhile the sample $x = 0.2$ calcined at the same temperature contains a mixture of α-Al_2O_3 and rutile. Therefore, the presence of small titanium amounts seems to facilitate the transformation into α-Al_2O_3 at temperatures below 900 C. This result is in agreement with those reported previously by other authors [39–43], who found that some oxides, such as Fe_2O_3, TiO_2, MgO, NiO, CuO, MnO_2, V_2O_5 and PtO promoted the transformation of γ-Al_2O_3 into α-Al_2O_3 at a temperature as low as 900 C. Additionally, the crystallization temperature of rutile for the $x = 0.2$ sample is lower than those found by Toba *et al.* [26] for two samples with the same composition prepared by simultaneous and separated hydrolysis of the two alkoxides (1034 and 961 C, respectively).

As it can be noticed, the formation of a crystalline phase seems to occur at lower temperatures while the titanium content increases. These observations are in agreement with the results reported by Inamura *et al.* [44] and by Klimova *et al.* [18] for the crystallization of ZrO_2-Al_2O_3 oxides. They observed that the crystallization process of the tetragonal zirconia phase occurred at higher temperatures while the aluminium content increased. Duchet *et al.* [45] also found an increase of 200 C in the crystallization temperature for ZrO_2 when it was doped with small amounts of Al_2O_3 (1–10 Al wt %).

4.4. Zero point charge (ZPC) values

In the mixed oxide systems, it is interesting to determine the surface distribution of the two oxides and its dependence upon the overall composition. The technique of electophoretic migration has proved to be very sensitive to variations in the surface coverage for a number of supported catalyst systems [46]. Wachs [47] found that under ambient conditions, where the surface was hydrated, the molecular structures of the surface metal oxide species were determined by the net pH at the zero point charge (ZPC) of the supported metal oxide system. Here, we consider that the ZPC of the mixed oxide will be the result of the contributions of the two oxides, and although this may not be essentially true in some cases, we will use it as an approximation to estimate the distribution of the two oxides on the surface of the mixed oxide. Accordingly, the decrease in the ZPC values relative to Al_2O_3 (isoelectric point -IEP- value of 7.2) will be due to the existence of a phase having an IEP lower than 7.2. Since in this case, TiO_2 has an IEP measured value of 3.8, the deviation from the line which goes through these two values, will be interpreted as variations in the composition of the surface. Besides, the ZPC values of the supports are of importance in the preparation of catalysts since for pH values above the zero point charge the surface of the support will be negatively charged, and conversely, for pH values below the ZPC the surface will be positively charged. Clearly, this will be of importance during the impregnation step of the active phase precursor salts where the active metals are present as cations or anions.

Fig. 6 shows the plot of ZPC vs. TiO_2 molar ratio. It can be seen that the values of ZPC for the mixed oxide samples are comprised between the values of the isoelectric point of the two simple oxides. The behaviour observed in the ZPC variations in all samples, with the

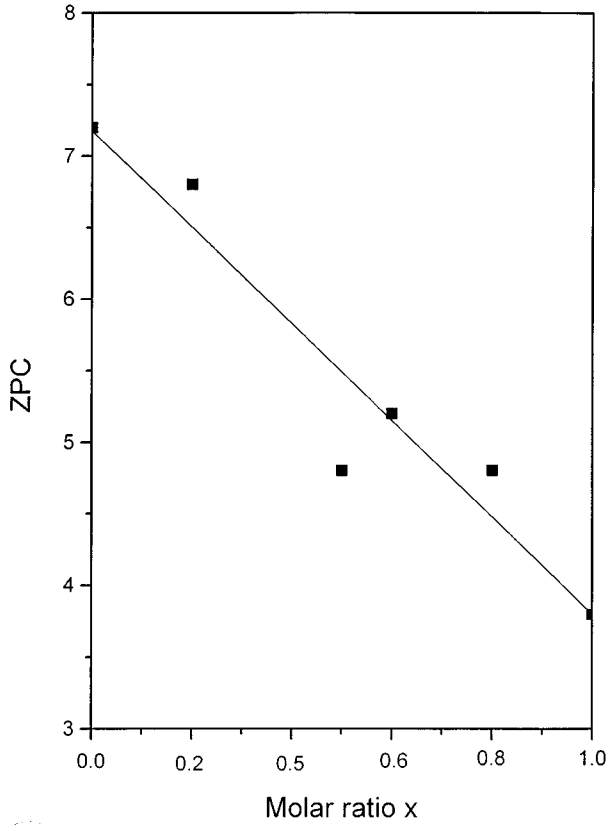

Figure 6 ZPC values of the samples of the $x\mathrm{TiO_2}\cdot(1-x)\mathrm{Al_2O_3}$ series calcined at 500 C.

exception of the $x = 0.5$ sample, is in good agreement with the equation:

$$\mathrm{ZPC}_{\mathrm{TiO_2\text{-}Al_2O_3}} = (\mathrm{IEP})_{\mathrm{TiO_2}}\cdot X_{\mathrm{TiO_2}} + (\mathrm{IEP})_{\mathrm{Al_2O_3}}\cdot X_{\mathrm{Al_2O_3}}$$

which relates the ZPC of the mixed oxide with the surface molar fraction (X) and isoelectric points (IEP) of the simple oxides (TiO_2 and Al_2O_3).

The linearity of the ZPC vs. X plot indicates that the surface distribution of titanium and aluminium oxides follows approximately the bulk composition of the corresponding mixed oxides, although this is not a complete proof of the homogeneity of the solids. In the case of $x = 0.5$, a considerable deviation of ZPC value with respect to the one expected from the straight line equation is observed, in such way that this sample has a ZPC value even lower than that corresponding to the $x = 0.6$ sample, which contains less aluminium amount. That is, the surface distribution of the $x = 0.5$ sample deviates from the expected for the bulk composition, and this fact could be attributed to a possible error in the preparation of this sample (the zeta potential measurements were repeated three times, obtaining the same value of ZPC for this sample). Other authors [18] also observed such deviation, although lower, for the $x = 0.5$ sample of the $x\mathrm{ZrO_2}\cdot(1-x)\mathrm{Al_2O_3}$ series. On the other hand, the IEP value obtained by us for the sample $x = 0$ is lower than that obtained by those authors for an alumina prepared in a similar way to ours, (although the calcination temperature and other conditions were different), and also lower than the one found by other authors [46] for a commercial γ-Al_2O_3 (8.8). However, we can not forget that in both reported cases the studied phase is γ-Al_2O_3, meanwhile in our case, the $x = 0$ sample calcined at 500 C is still amorphous (as shown in the corresponding difractogram of Fig. 4); therefore, it is logical that the surface characteristics of the samples are also different. Similarly, the IEP value (3.8) for TiO_2 ($x = 1.0$) obtained by us is also considerably lower than the one measured by other authors [46] for a commercial TiO_2 sample from Degussa (6.3), which indicates the different surface characteristics of both samples, the commercial and the prepared by the sol-gel method.

4.5. Surface acidity

The acidity of alumina-titanias, which is one of the important factors controlling the catalysis, can vary with the preparation method for the following reasons. The acidity of mixed oxides has been generally considered to result from an excess of negative or positive charge caused by the formation of bridged hetero metal-oxygen bonds (M-O-M′) [48]. In a mixed oxide containing M and M′ metals, the degree of M-O-M′ bond formation depends on the degree of mixing of M and M′, namely the homogeneity of the mixed oxide which changes with the preparation methods. On the other hand, in many catalytic systems, the support not only allows a high dispersion of the active phase, but also plays a role in determining the catalytic activity and some explanations of this effect can be given in term of carrier acidity. For these reasons, it is very important to determine the acidity of the mixed oxides which will be used as supports for a determined catalytic system.

As indicated in the experimental section, a potentiometric method of titration with *n*-butylamine was used to characterize the surface acidity [19]. The titration curves for the samples of the $x\mathrm{TiO_2}\cdot(1-x)\mathrm{Al_2O_3}$ series calcined at 500 C are plotted in Fig. 7. Table IV shows the values of the initial electrode potential (E_0) as well as the potential decreasing (ΔV) produced during the titration. According to the method used, the initial electrode potential indicates the maximum acid strength of the first titrated surface acid sites. Therefore, it can be observed that the maximum acid strength increases with the molar ratio of TiO_2 up to $x = 0.6$, decreasing for samples with higher values of x. That is, the sample $x = 0.6$ seems to contain the combination of Al-Ti acid sites with highest acid strength. It can be also noticed that when the TiO_2 molar ratio is small ($x = 0.2$), the acid strength of the strongest acid sites almost does not change with regard to that of the sample containing only alumina ($x = 0.0$). In this way, the initial potential values are very similar and both titrations curves practically overlap. However, when the titanium content increases up to $x = 0.5$, an increment of 40 mV in the E_0 value is produced, which indicates that stronger acid sites are generated. This increase of the E_0 value

TABLE IV Results of the titration with *n*-butylamine for the samples of the $x\mathrm{TiO_2}\cdot(1-x)\mathrm{Al_2O_3}$ series, calcined at 500 C

Sample	$x = 0.0$	$x = 0.2$	$x = 0.5$	$x = 0.6$	$x = 0.8$	$x = 1.0$
E_0 (mV)	−147	−144	−106	136	44	−76
ΔV (mV)	99	96	100	297	207	105

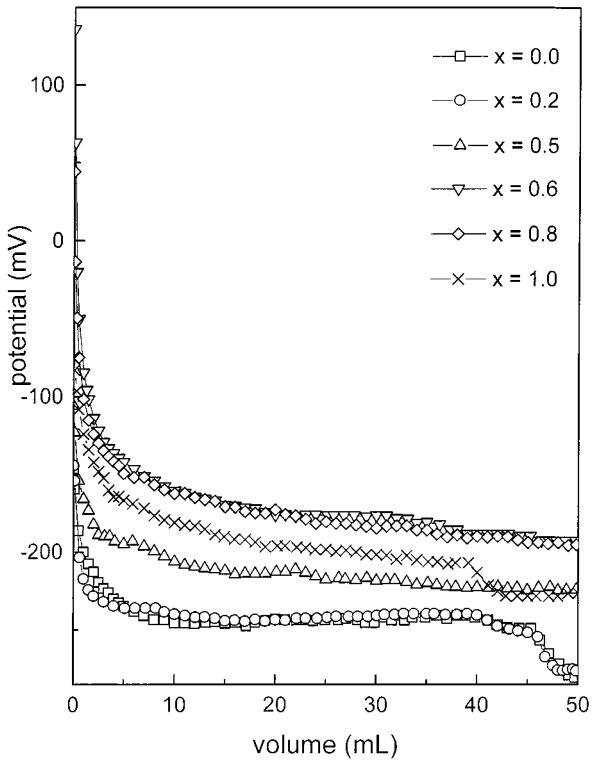

Figure 7 Titration curves with *n*-butylamine for the samples of the $x\mathrm{TiO_2}\cdot(1-x)\mathrm{Al_2O_3}$ series calcined at 500 C.

is more substantial for the sample $x = 0.6$, in such way that this sample shows the highest E_0 value. Therefore, as explained before, this sample contains the combination of Al-Ti acid sites with highest acid strength, showing its titration curve above all the others. When the titanium content continues increasing ($x = 0.8$, $x = 1.0$), the maximum acid strength of the first titrated surface acid sites decreases again (a decrease of the E_0 value is observed). These results are in line with those reported by Shibata *et al.* [49] in the sense that the acid strength of a mixed oxide is generally higher than those of the component oxides, because a stronger acid site is generated by the formation of bridged hetero metal-oxygen bonds (M-O-M′). The higher the miscibility or formation of these hetero bonds the higher is the acid strength.

On the other hand, the higher the potential decrease produced during the titration, the higher is the difference of acidity between the initial and final acid sites of each step of the titration curve. Conversely, very small potential decreases indicate a very similar acid strength between both types of acid sites. Thus, most of the samples of the $x\mathrm{TiO_2}\cdot(1-x)\mathrm{Al_2O_3}$ series seems to have a very similar distribution of acid sites, because the potential decrease produced is almost the same in all cases (around 100 mV), except for the $x = 0.6$ and $x = 0.8$ samples, which show a potential decrease three times and twice higher, respectively. For the samples $x = 0.0$ and $x = 0.2$, besides of a first plateau reached around 10 mL, a second step in the titration curve is observed after the addition of approximately 45 mL, which seems to indicate the existence of two types of acid sites in these two samples. Something similar occurs in the titration of sample $x = 1.0$, which experiments a second fall in the titration curve after 39 mL.

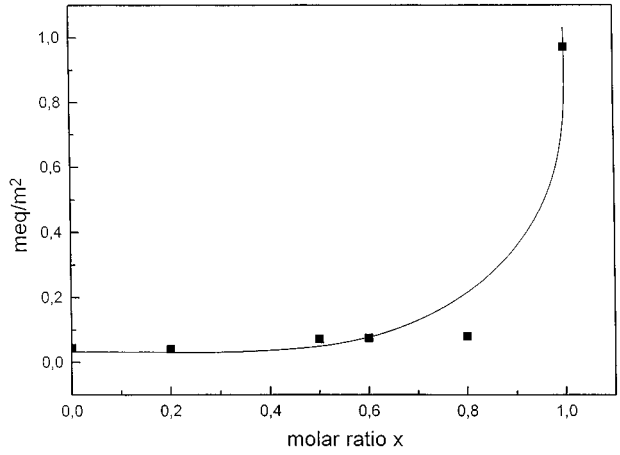

Figure 8 Acid sites surface density for the samples of the $x\mathrm{TiO_2}\cdot(1-x)\mathrm{Al_2O_3}$ series calcined at 500 C.

It can be observed that the volume of basic solution added to get the first plateau on the titration curve increases with the molar ratio of $\mathrm{TiO_2}$, in such way that the curves of the $x = 0.6$, $x = 0.8$ and $x = 1.0$ samples seem not to get the plateau completely in the studied range, but they show a slow and continuous fall. This means that the distribution of acid sites is wider for the samples with higher titanium content, meanwhile the samples with a low content of this element ($x = 0.0$, $x = 0.2$) seem to contain a narrow energetic distribution of acid sites: the strongest ones titrated firstly until a consumption of about 10 mL, and other weaker neutralizated after 45 mL. This is in agreement with the results observed by other authors for $\mathrm{TiO_2}\cdot(1-x)\mathrm{Al_2O_3}$ supports [25]. They found that the number of weak and strong acid sites in the mixed oxides was almost the same that for the pure alumina, meanwhile the number of acid sites of medium strength increased linearly with the titanium content.

From the potential values at the plateau (determined in some cases by extrapolation), the number of miliequivalents of amine consumed has been calculated, and as the surface area of each sample is known, the acid sites surface density has been also calculated. The results are shown in Fig. 8. It can be observed that when the titanium content of the mixed oxides increases, a continuous increment of the acid sites density is produced, being much more pronounced for the sample containing only titania. These results are in good agreement with those reported previously by Centi *et al.* [50] and by Klimova *et al.* [18] for $\mathrm{ZrO_2}$-$\mathrm{Al_2O_3}$ mixed oxides. These last authors observed that acid sites density increased only slightly with the incorporation of zirconia to the alumina, and that increased substantially for the pure zirconia sample. Clearly, all the results presented about strength and distribution of acid sites are very interesting since they show the possibility of tuning the surface acidity of the mixed oxides which will be used as supports for hydrotreating reactions.

5. Summary and conclusions

A series of $x\mathrm{TiO_2}\cdot(1-x)\mathrm{Al_2O_3}$ mixed oxides with different molar ratios has been prepared by the sol-gel method. This method has allowed us to obtain Ti-Al

mixed oxides with higher surface area than alumina and titania, hence making these solids interesting as catalytic supports. In addition, it is possible to tune to some extent the pore size distribution of the mixed oxide by changing its composition. Thus, the presence of titanium in the calcined samples until a ratio of $x = 0.5$ leads to the formation of smaller pores than those formed in the alumina sample. The crystallization process induced by calcination occurs at temperatures higher than 500 C for the $0.0 \leq x \leq 0.6$ samples. This crystallization process is shifted to higher temperatures when the aluminium content increases. On the other hand, the presence of titania in the Ti-Al mixed oxides promotes the formation of α-Al_2O_3. The samples rich on aluminium ($x = 0.0$, $x = 0.2$) contain crystalline phases of aluminium compounds, while the diffractograms of the samples with high molar ratios of TiO_2 show the presence of titanium compounds. The ZPC results indicate the formation of a surface composition equivalent to the bulk composition of the two oxides. The acid sites surface density, as determined by *n*-butylamine titration, increases with titania content, allowing the tuning of the acid properties of the mixed oxide supports. Furthermore, the strength of the acid sites may be varied by changing the composition of the mixed oxide, being the $x = 0.6$ sample the one containing the combination of Ti-Al acid sites with highest acid strength.

References

1. M. BREYSSE, J. L. PORTEFEIX and M. VRINAT, *Catal. Today* **10** (1991) 489.
2. W. ZHAOBIN, X. QUIN, G. XIEXIAN, E. L. SHAM, P. GRANGE and B. DELMON, *Appl. Catal.* **63** (1990) 305.
3. F. LUCK, *Bull. Soc. Chim. Belg.* **100** (1991) 781.
4. T. LÓPEZ, A. ROMERO and R. GOMEZ, *J. Non-Cryst. Solids* **127** (1991) 105.
5. K. BALAKRISHNAN and R. D. GONZÁLEZ, *J. Catal.* **144** (1993) 395.
6. A. Z. KHAN and E. RUCKENSTEIN, *Appl. Catal.* **90** (1992) 199.
7. M. L. ROJAS-CERVANTES, A. J. LÓPEZ-PEINADO, J. DE D. LÓPEZ-GONZÁLEZ and F. CARRASCO-MARÍN, *J. Mater. Sci.* **31** (1996) 437.
8. L. LEBIHAN, C. MAUCHAUSSÉ, L. DUHAMET, J. GRIMBLET and E. PAYENT, *J. Sol-Gel Sci. Tecn.* **2** (1994) 837.
9. J. RAMIREZ, R. CUEVAS, P. CASTILLO, M. L. ROJAS and T. KLIMOVA, *Bulg. Chem. Commun.* **30**(1/2) (1998) 207.
10. I. C. WEISSMAN, E. I. KO and S. KAYTAL, *Appl. Catal.* **94** (1993) 45.
11. S. MATSUDA and A. KATO, *ibid.* **8** (1983) 149.
12. K. FOGER and J. R. ANDERSON, *ibid.* **23** (1986) 139.
13. Z. B. WEI, Q. XIN, X. X. GUO, E. L. SHAM, P. GRANGE and B. DELMON, *Appl. Catal.* **83** (1990) 305.
14. H. TAMARA, M. BOULINGUIEZ and M. VRINAT, *Catal. Today* **29** (1996) 209.
15. K. SEGAWA, M. KATSUTA and F. KAMEDA, *ibid.* **29** (1996) 215.
16. J. RAMIREZ, L. RUIZ-RAMIREZ, L. CEDEÑO, V. HARLE, M. VRINAT and M. BREYSSE, *Appl. Catal.* **93** (1993) 163.
17. M. L. ROJAS-CERVANTES, R. M. MARTÍN-ARANDA, A. J. LÓPEZ-PEINADO and J. DE D. LÓPEZ-GONZÁLEZ, *J. Mater. Sci.* **29** (1994) 3743.
18. T. KLIMOVA, M. L. ROJAS, P. CASTILLO, R. CUEVAS and J. RAMIREZ, *Microporous Mesoporous Mater.* **20** (1998) 293.
19. R. CID and G. PECCHI, *Appl. Catal.* **14** (1985) 15.
20. M. DEEBA and W. K. HALL, *J. Catal.* **60** (1979) 417.
21. B. C. LIPPENS and J. H. DE BOER, *ibid.* **4** (1965) 319.
22. E. P. BARRET, L. S. JOYNER and P. P. HALLENDA, *J. Am. Chem. Soc.* **73** (1952) 373.
23. G. HORVARTH and K. KAWAZOE, *J. Chem. Eng. Japan* **16**(6) (1983) 470.
24. T. KLIMOVA, Y. HUERTA, M. L. ROJAS-CERVANTES, R. M. MARTÍN-ARANDA and J. RAMIREZ, in "Studies in Surface Science and Catalysis, Vol. 91," edited by G. Poncelet, J. Martens, B. Delmon, P. A. Jacobs and P. Grange (Elsevier, Amsterdam, 1995) p. 411.
25. E. OLGUIN, M. VRINAT, L. CEDEÑO, J. RAMIREZ, M. BOSQUE and A. LÓPEZ-AGUDO, *Appl. Catal. A* **165** (1997) 1.
26. M. TOBA, F. MIZUKAMI, S. I. NIWA, Y. KIYOZUMI, K. MAEDA, A. ANNILA and V. KOMPPA, *J. Mater. Chem.* **414** (1994) 585.
27. J. RAMIREZ and A. GUTIERREZ-ALEJANDRE, *J. Catal.* **170** (1997) 108.
28. H. L. LEE and H. S. LEE, *J. Mater. Sci. Lett.* **13** (1994) 316.
29. J. P. OLIVIER, *J. Porous Mater.* **2** (1995) 9.
30. I. A. MONTOYA, T. VIVEROS, J. M. DOMINGUEZ, L. A. CANALES and I. SCHIFTER, *Catal. Lett.* **15** (1992) 207.
31. I. GASIOR, M. GASIOR, B. GRZYBOWSKA, R. KOZLOWSKI and J. SLOCZYNSKI, *Bull. Acad. Pol. Sci.* **27** (1979) 829.
32. R. Y. SALEH, I. E. WACHS, S. S. CHAN and C. C. CHERSICH, *J. Catal.* **98** (1986) 102.
33. V. A. NIKOLOV and A. I. ANASTASOV, *Ind. Eng. Chem. Res.* **31** (1992) 80.
34. Z. H. SUO, Y. KOU, J. Z. NIU, W. Z. ZHANG and H. L. WANG, *Appl. Catal. A* **29** (1997) 4913.
35. X. FU, W. A. ZELTNENJR, Q. YANG and M. ANDERSON, *J. Catal.* **168** (1997) 482.
36. R. A. SPURR and H. MYERS, *Anal. Chem.* **29** (1957) 760.
37. B. C. LIPPENS and J. H. DE BOER, *Acta Crystallogr.* **17** (1964) 1312.
38. H. S. SANTOS and P. S. SANTOS, *Mater. Lett.* **13** (1992) 175.
39. Y. WAKAO and T. HIBINO, *Nagoya Kogyo Gijutsu Schimanko Hokoku* **11** (1962) 588.
40. G. C. BYE and G. T. SIMPKIN, *J. Am. Ceram. Soc.* **57** (1974) 367.
41. N. S. KURKOVA, Y. R. KATSOBASHVILI and N. A. AKCHURINA, *Zh. Prikl.* **46** (1973) 1002.
42. N. S. KOZLOV, M. Y. LAZAREV, L. MOSTOVAYA and I. P. STREMOK, *Kinet. Catal.* **14** (1973) 1130.
43. a) P. BURTIN, J. P. BRUNELLE, M. PIJOLAT and M. SOUSTELLE, *Appl. Catal.* **24** (1987) 239; b) *ibid.* **34** (1987) 225.
44. S. INAMURA, H. MIYAMOTO, Y. IMAIDA, M. TAKAGAWA, K. HIROTA and O. YAMAGUCHI, *J. Mater. Sci.* **29** (1994) 4913.
45. J. C. DUCHET, M. J. TILLIETTI and D. CORNET, *Catal. Today* **10** (1991) 98.
46. a) F. J. GIL-LLAMBÍAS and A. M. ESCUDEY CASTRO, *J. Chem. Soc. Chem. Commun.* (1982) 478; b) F. J. GIL-LLAMBÍAS, A. M. ESCUDEY CASTRO, A. LÓPEZ AGUDO and J. L. G. FIERRO, *J. Catal.* **90** (1984) 323; c) F. J. GIL-LLAMBÍAS, A. M. ESCUDEY CASTRO, J. L. G. FIERRO and A. LÓPEZ AGUDO, *ibid.* **95** (1985) 520.
47. I. E. WACHS, *Catal. Today* **27** (1996) 437.
48. K. TANABE, T. SUMIYOSHI, K. SHIBATA, T. KIYOURA and J. KITAGAWA, *Bull. Chem. Soc. Jpn.* **47** (1974) 1064.
49. K. SHIBATA, T. KIYOWA, J. KITAGAWA, T. SUMIYOSHI and K. TANABE, *ibid.* **46** (1973) 2985.
50. G. CENTI, M. MARELLA, L. MEREGALLI, S. PERATHONER, M. TOMASELLI, T. LA TORRETA, in "Advances Catalysts and Nanostructured Materials," edited by W. R. Moser (Academic press, New York, 1996) p. 63.

Received 27 May
and accepted 18 November 1999